Batch fabrication of nanopatterned graphene devices via nanoimprint lithography

Mackenzie, David; Smistrup, Kristian ; Whelan, Patrick Rebsdorf; Luo, Birong; Shivayogimath, Abhay; Nielsen, Theodor; Petersen, Dirch Hjorth; Messina, Sara A.; Bøggild, Peter

Published in:
Applied Physics Letters

Link to article, DOI:
10.1063/1.5010923

Publication date:
2017

Document Version
Publisher's PDF, also known as Version of record

Batch fabrication of nanopatterned graphene devices via nanoimprint lithography

David M. A. Mackenzie, Kristian Smistrup, Patrick R. Whelan, Birong Luo, Abhay Shivayogimath, Theodor Nielsen, Dirch H. Petersen, Sara A. Messina, and Peter Bøggild

Citation: Appl. Phys. Lett. **111**, 193103 (2017);
View online: https://doi.org/10.1063/1.5010923
View Table of Contents: http://aip.scitation.org/toc/apl/111/19
Published by the American Institute of Physics

Batch fabrication of nanopatterned graphene devices via nanoimprint lithography

David M. A. Mackenzie,[1,2,a)] Kristian Smistrup,[3] Patrick R. Whelan,[1,2] Birong Luo,[4,b)] Abhay Shivayogimath,[1,2] Theodor Nielsen,[3] Dirch H. Petersen,[1,2] Sara A. Messina,[1,2] and Peter Bøggild[1,2]

[1]*Department of Micro- and Nanotechnology, Technical University of Denmark, Ørsteds Plads 345 B, 2800 Kongens Lyngby, Denmark*
[2]*Center for Nanostructured Graphene (CNG), Technical University of Denmark, DK-2800 Kongens Lyngby, Denmark*
[3]*NIL Technology APS, Diplomvej 381, DK-2800 Kongens Lyngby, Denmark*
[4]*Cambridge Graphene Centre, Engineering Department, University of Cambridge, 9 JJ Thomson Avenue, Cambridge CB3 0FA, United Kingdom*

(Received 27 April 2017; accepted 26 October 2017; published online 8 November 2017)

Previous attempts to tune the electrical properties of large-scale graphene *via* nanopatterning have led to serious degradation of the key electrical parameters that make graphene a desirable material for electronic devices. We use thermal nanoimprint lithography to pattern wafer-scale graphene on a 4-in. wafer with prefabricated 25 mm^2 devices. The nanopatterning process introduces a modest decrease in carrier mobility and only a minor change in residual doping. Due to the rapid fabrication time of approximately 90 min per wafer, this method has potential for large-scale industrial production. The chemiresistive gas sensing response towards NO_2 was assessed in humid synthetic air and dry air, with devices showing a response to 50 ppb of NO_2 only when nanopatterned.

https://doi.org/10.1063/1.5010923

Since initial excitement regarding the isolation of graphene,[1] many groups have successfully modified the properties of graphene *via* chemical or physical modification. One such strategy is to use nanopatterning to create either a transport gap[2] for use in transistors or to create adsorption sites for gas sensors.[3] Previous nanopatterning methods have used electron beam lithography (EBL)[4] or block-copolymer (BCP)[3] lithography to pattern etch masks. However, the inherent serial nature of EBL imposes a severe limit to the overall throughput, which presents a challenge in terms of upscaling for industry applications. On the other hand, BCP lithography has the theoretical capability to provide wafer-scale self-assembling nanostructures from a polymer spin-on process but is technically very difficult to realise without significant wafer-to-wafer reproducibly issues and local spatial variability issues. In contrast, nanoimprint lithography (NIL) masks can be fabricated using a single EBL exposure and then reused.[5] Once the NIL mask is fabricated, nanopatterned graphene can be produced with the extraordinary pattern density of EBL.[4] In combination with the well-established fast and reliable throughput and low cost of ownership of NIL, this seems to be ideal for upscaling to commercial production.

In early demonstrations of NIL nanopatterning of exfoliated graphene,[6] the electrical properties were significantly affected compared to the results obtained with as-exfoliated graphene. Here, we present an approach that combines NIL with a laser-ablation method we introduced earlier,[7] which converts a 4-in. silicon wafer with a transferred single-layer chemical vapor deposited graphene sheet into (5 mm × 5 mm) electrical devices with sub-100 nm nanopatterning. We show that that these devices are subject to relatively weak perturbations of the electrical properties, while providing the expected enhancement of the gas sensing response, in the role of a chemiresistive gas sensor device.

Figures 1(a)–1(d) show a schematic of our fabrication process for millimetre-sized devices. Initially, electrodes of 5 nm Cr/45 nm Au were defined *via* a shadow mask using electron beam evaporation onto a 100 mm diameter silicon wafer with a top passivation layer of 300 nm SiO_2, as shown in Fig. 1(a). Then, wafer-scale graphene was grown[8] at 1000 °C on electropolished copper foil of 25 μm thickness[9] optimized for single-layer growth[10] and transferred by standard processes,[11,12] resulting in graphene covering the entire wafer with prefabricated electrodes, as shown in Fig. 1(b). Figure 1(c) illustrates how the graphene devices were defined *via* selective laser ablation,[7] which leaves the electrical properties of graphene unaffected.[13] The above processing steps are designed to minimize contact with solvents/water as well as to avoid resist residues, which are known to degrade electrical parameters of graphene[14] and which can interfere with the following imprint processing steps. The devices are immediately ready for electrical characterization; these measurements may be used as a quality control step before NIL so that further processing is only implemented on wafers/devices of sufficient quality/homogeneity, as previously defined in Ref. 15. Figures 1(e)–1(h) show the NIL process, which was performed using a CNI v2.0 imprint tool from NIL Technology. We began by spinning 85 nm mr-I

a)Author to whom correspondence should be addressed. Electronic mail: dmac@nanotech.dtu.dk
b)This research was performed while B. Luo was at the Center for Nanostructured Graphene (CNG), Technical University of Denmark, DK-2800 Kongens Lyngby, Denmark.

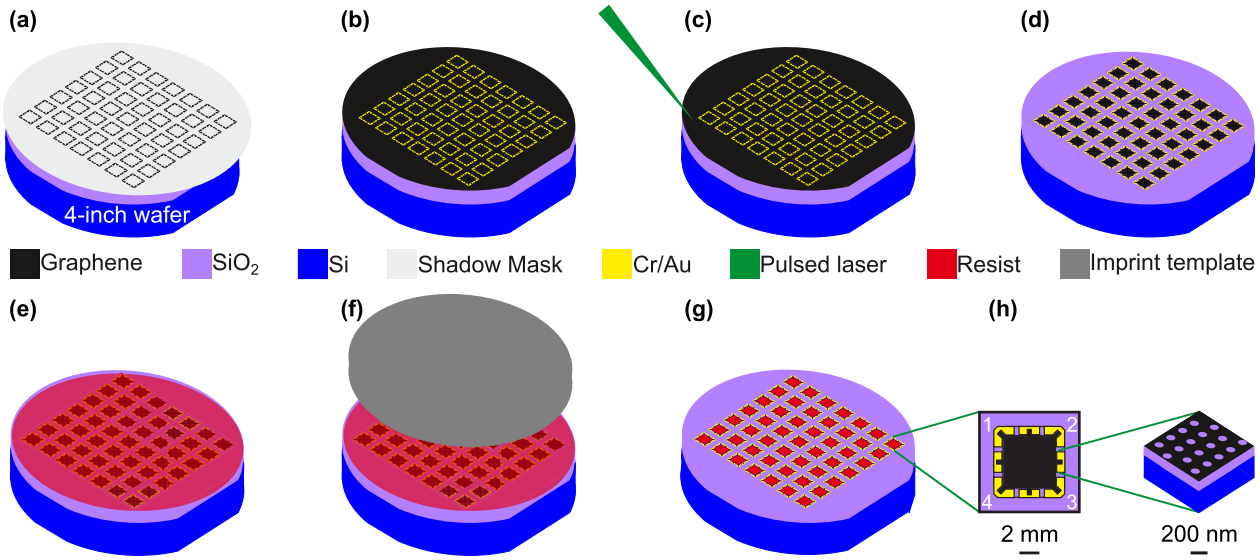

FIG. 1. Schematic of device fabrication. (a) Electrodes of 5 nm Cr and 45 nm Au were deposited through a shadow mask onto a 4-in. wafer with 300 nm SiO_2. (b) A single sheet of graphene is transferred to an entire wafer. (c) A pulsed laser selectively ablates graphene[7] to define individual devices. (d) Devices are ready for pre-nanopatterned measurements. (e) NIL-compatible resist is spun onto the wafer. (f) NIL processing. (g) Reactive ion etching defines the nanopattern, followed by the removal of resist. (h) Overview of individual 5 mm × 5 mm devices, with the inset illustrating a magnified view of the patterned area.

7010E resist at 1750 rpm for 60 s [see Fig. 1(e)]. The NIL master was created using a JEOL JBX-9500 electron beam lithography system and consists of multiple 5 mm × 5 mm patterned device areas, with a center-to-center distance between the devices of 10 mm. The pattern was imprinted at a temperature of 130 °C and a pressure of 6 bars for 10 min [Fig. 1(f)]. A reactive ion etch with a mixture of 2 sccm of O_2 and 20 sccm of N_2 with an RF power of 20 mW was performed to define the pattern, as shown in Fig. 1(g). Although the pitch of our NIL mask is constant, some control over the neckwidth was achievable by varying the etching time compared to the default time of 60 s. Finally, the resist was removed in warm acetone. Figure 1(h) shows a single 5 mm × 5 mm device with numbered electrodes, with the close-up indicating the nanopattern.

Electrical measurements were performed using dual configurations, i.e., with two different current-voltage probe configurations on the device. Following the notation in Fig. 1(h): Configuration A (Source = 1, Drain = 2, $V_+ = 4$, $V_- = 3$) and configuration C (Source = 2, Drain = 3, $V_+ = 1$, $V_- = 4$) are used to determine the resistances R_A and R_C, from which the sheet resistance R_{vdP} can be calculated using the following formula[16]

$$e^{-\frac{\pi R_A}{R_{vdP}}} + e^{-\frac{\pi R_C}{R_{vdP}}} = 1.$$

Two Keithley 2400 source-measure units provided the supplied and measured current, with voltage measurements performed using a Keithley 2700 and multiplexing switching performed using a Keithley 7705. Electrical measurements were carried out in dry nitrogen at 30 °C as described in Ref. 14.

Raman spectroscopy maps were obtained using a Thermo Scientific DXRxi Raman spectrometer with a 532 nm laser at 3 mW, a collection time of 5.5 ms, and a pixel density of 100 mm^{-2} and analyzed following Ref. 17.

Gas sensing measurements were performed using a Linkam LN600P heated, gas-tight probe station combined with a MTI GSL-LCD-4Z mass flow controller system and a standard bubbler with deionized water for controlling humidity. Prior to each measurement, the device was thermally annealed at 150 °C for 2 min in order to degas adsorbents and subsequently allowed to thermally stabilize at the measurement temperature for 5 min. All gases were diluted in dry synthetic air of purity 99.999% with the gas flow input to the measurement chamber kept at 100 sccm at all times.

The devices were measured before [as in Fig. 1(d)] and after NIL [as shown in Fig. 1(h)], with a measurement example shown in Fig. 2(a). Here, we observe an increase in sheet resistance at the charge neutrality point (CNP) from 6.2 kΩ to 26 kΩ and a decrease in carrier mobility from 2.3×10^3 cm^2/Vs to 4.5×10^2 cm^2/Vs; this is the largest change observed in any of the studied devices. The horizontal position of the CNP changes slightly from −1.5 V to 0.5 V, corresponding to a change in the carrier density n of 1.4×10^{11} cm^{-2}. These modest changes in mobility and doping seem to be a considerable improvement from the significant degradations of previous methods for dense nanopatterning[4,6,18] where a reduction in the mobility of over a factor of 10^2–10^4 has typically been reported.

Figure 2(b) shows, for the device shown in Fig. 2(a), scanning electron microscopy (SEM) images of representative regions of the nanopatterned graphene. The pattern is uniform and extends across the entire device area of 5 mm × 5 mm except for relatively small regions with minor irregularities. Such pattern artefacts are often attributed to dust/defects, which affects the local NIL pattern transfer. Only a few resist residues were visible across the devices, which may partially explain the relatively small change in doping after NIL processing in our devices.[14] Our specific NIL mask has four distinct 5 mm × 5 mm areas with a pitch/neckwidth [as defined in Fig. 2(d) inset)] of 200 nm/100 nm, 200 nm/120 nm, 200 nm/140 nm, or 300 nm/160 nm. This leads to a total number of holes per device of 6.25×10^6 (pitch 200 nm) or 0.28×10^6 (pitch 300 nm).

Large-area Raman spectroscopy maps of 5000 spectra were recorded for devices before [as shown in Fig. 1(d)] and

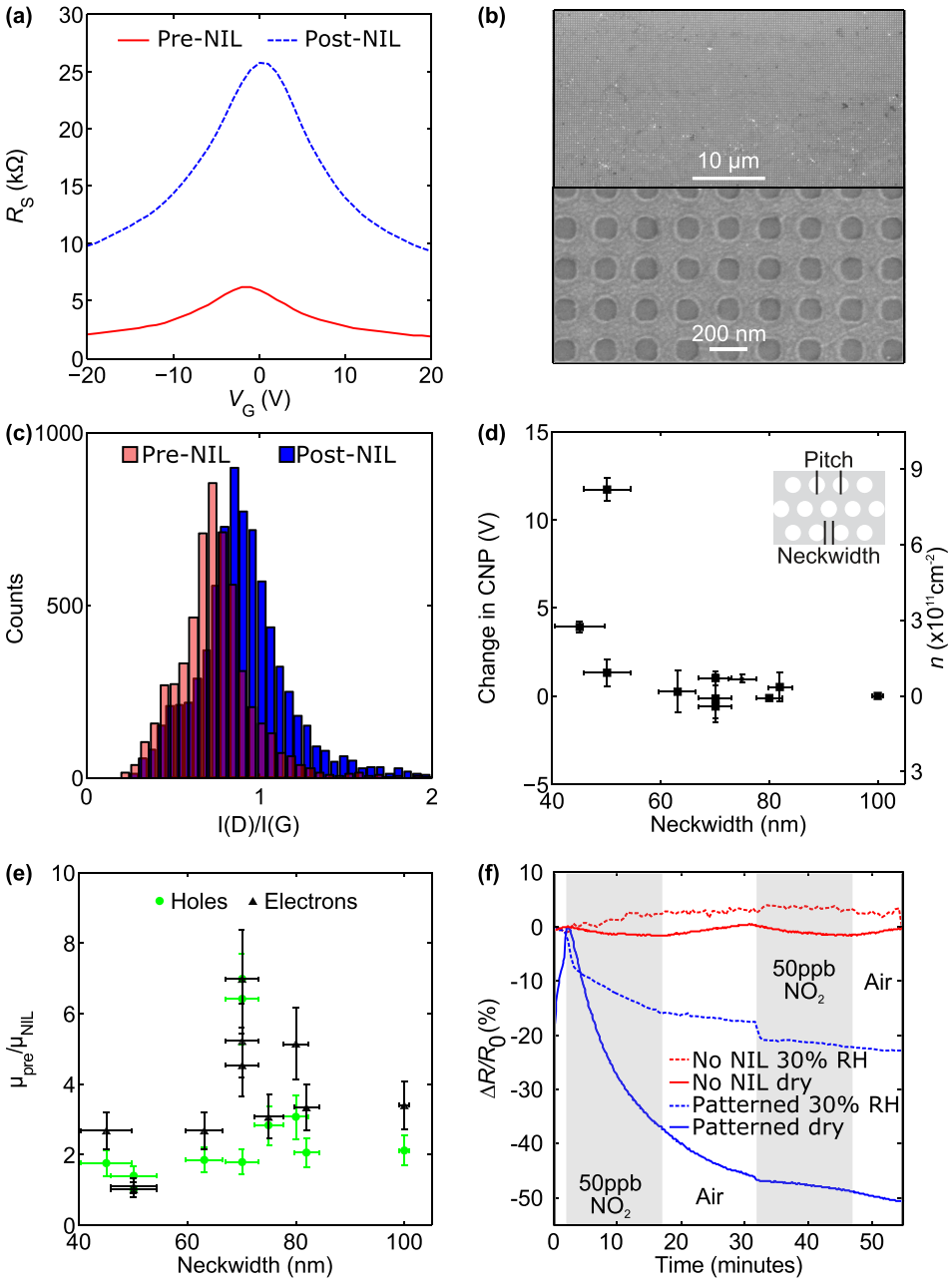

FIG. 2. (a) Sheet resistance (R_S) as a function of gate bias (V_G) for a typical device before processing (solid line) and after (dashed line) NIL processing. (b) Scanning electron micrograph of part of the device shown in (a). (c) Histogram of Raman spectroscopy data showing the ratio, I(G)/I(D), of the G-peak to D-peak intensities, both before (blue) and after (red) NIL processing. (d) Change in doping as a result of NIL processing. (e) Carrier mobility decrease due to NIL processing for holes (green circles) and electrons (black triangles). (f) Gas measurements comparing patterned (blue lines) and non-patterned (red lines) devices, conducted in ambient conditions with 30% relative humidity (solid lines) or in dry conditions (dashed lines), with 2 min of air flow, followed by alternating 15 min environments of 50 ppb NO_2 and air.

after processing [as shown in Fig. 1(h)] to assess any changes in defect density. The measured intensity ratio I(D)/I(G) of the D- and G-peaks is a qualitative coverage-independent measure of lattice defects and sp^3 bond density in graphene.[19] Histograms showing I(D)/I(G) for device 1 before and after NIL are shown in Fig. 2(c), where only a slight increase in the mean of I(D)/I(G) from 0.75 to 0.93 is observed for device 1 after processing. A small increase in I(D)/I(G) suggests that the NIL resist protects the graphene well from the etching process and that any defects present in the nanopatterned devices are mainly attributable to factors induced prior to fabrication (i.e., from growth and transfer).

The change in doping density was $10^{12}\,\mathrm{cm}^{-2}$ or less for all ten devices as shown in Fig. 2(d), and for all but one of the devices, an increase in p-doping was observed. The slight increase defect density is consistent with our observation of only a small decrease in carrier mobility.[19] Statistical uncertainties in carrier doping and mobility were calculated from the variation between the calculated vdP values and the A and C configurations, as described in Ref. 15, taking into account that the uncertainty of the neck-width was determined from SEM images. The neck-width is defined in Fig. 2(d), inset. In Fig. 2(e), the relative decrease in mobility is shown for all samples, with a factor of 5 representing the worst case, also shown in Fig. 2(a). There are several possibilities for the small doping level compared to what is typically observed by PMMA-based electron beam lithography, which was for instance found to be of order $3–7 \times 10^{12}\,\mathrm{cm}^{-2}$ for graphene antidot lattices with neckwidths comparable to ours.[20] NIL-based lithography avoids irradiating the sample by electrons, which is known to cause detrimental effects in graphene devices.[20] For high density patterns, near contacts and edges and for miniaturized devices, elastic and inelastic electron scattering effects can lead irradiation outside the areas intended for patterning. These stray electrons can not only cause unwanted proximity effects and pattern distortion

but also cause direct damage to the graphene at electron energies well below the 85 keV threshold for knock-on damage.[21,22] The most frequently used and studied positive electron beam resist in graphene research, PMMA, is not only chain-scissioned but also cross-linked under electron beam irradiation, which would make residues less soluble and ultimately increase doping levels compared to NIL. Moreover, the carrier mobility can also be reduced in patterned areas,[23] and since the patterns in samples such as ours are fairly dense, we attribute the low level of doping and defect generation to the avoidance of electron beam irradiation.

One of the most well-established applications of nanopatterned graphene is for the enhancement of the chemiresistive gas sensing response. To assess the chemiresistive response for the fabricated structures against typical results from nanopatterned graphene devices in the literature, we performed gas sensing measurements. The chemiresistive response to 50 ppb NO_2 gas is shown in Fig. 2(f) for both dry and ambient conditions with approximately 30% relative humidity (RH). We observe a significant response to NO_2 only after nanopatterning, consistent with previous measurements on nanopatterned graphene.[3] Llobet[24] suggested that the edges of graphene patterns act as adsorption sites, which can both change the average time the reagents spend in contact with the device and enhance charge transfer. In all gas sensing measurements, the graphene was initially p-doped. Electrons transferred from the device to NO_2 caused further p-doping, as seen from the measured decrease in $\Delta R/R_0$. We note a lack of recovery when NO_2 flow was terminated and significant drift of the resistance, which we attribute to the abovementioned enhanced binding of adsorbed molecules on edges of the nanopatterned devices.[25] This is consistent with our observation of the smaller response for the second NO_2 injection. We found that the sensor could be reset with a 2 min anneal at 150 °C and that it likely that measurements performed at higher temperature could allow for accelerated desorption under neutral gas conditions and thus faster recovery. In a humid atmosphere, conventional solid-state gas sensors are known to be affected in several ways.[26–28] For our nanopatterned graphene sensors, we observe a decreased response in the presence of humidity, while for non-patterned graphene, the introduced noise was sufficient to obscure any gas response. We note that even in the humid atmosphere, NO_2 levels below the EU inhalation limits[29] were detected with the nanopatterned devices, which underpins the potential of efficient, large-area nanopatterning methods as a route to better, real-world graphene-based gas sensors.

We demonstrate a fast route to large-area nanopatterned graphene devices with remarkably low levels of defect generation and doping, as shown by electrical and Raman spectroscopy data collected before and after NIL processing. We attribute the low level of degradation of the electrical properties to the entire process flow which is designed to minimize device exposure to polymers, solvents, and electron irradiation, achieved by the combination of shadow masking, laser ablation, and NIL. Our fabrication method combines laser ablation, nanostencil-based metal deposition, and nanoimprint lithography, to provide a complete large-area nanopatterning and device fabrication approach, with excellent throughput (90 min for a 100 mm wafer). While the task of patterning the mask may still be time-consuming, once the mask is created, it can be used hundreds of times. Moreover, an inverse master stamp can be used to create multiple copies (potentially used in parallel), in effect eliminating the start-up cost for larger production scenarios. To demonstrate that the nanopatterned devices behave as expected, they were operated as gas sensors operating in ambient air, detecting NO_2 below the EU inhalation limits.

We thank the Nanocarbon Group at DTU Nanotech for useful discussions as well as the staff at DTU Danchip for valuable fabrication guidance. Regarding funding, we would like to recognize DNRF103 CNG, HC Ørsteds foundation, Villum Fonden Project No. VKR023117, the DA-GATE Project (No. 12-131827), and EC Graphene FET Flagship Contract No. 604391. This has received funding from the EU Horizon 2020 research and innovation programme under Grant Agreement No. 696656.

[1]K. S. Novoselov, A. K. Geim, S. V. Morozov, D. Jiang, Y. Zhang, S. V. Dubonnos, I. V. Grigorieva, and A. A. Firsov, "Electric field effect in atomically thin carbon films," Science **306**, 666–669 (2004).
[2]T. Gunst, T. Markussen, A. Jauho, and M. Brandbyge, "Thermoelectric properties of finite graphene antidot lattices," Phys. Rev. B **84**, 155449 (2011).
[3]A. Cagliani, D. M. A. Mackenzie, L. K. Tschammer, F. Pizzocchero, K. Almdal, and P. Bøggild, "Large-area nanopatterned graphene for ultrasensitive gas sensing," Nano Res. **7**(5), 743–754 (2014).
[4]D. M. A. Mackenzie, A. Cagliani, L. Gammelgaard, B. S. Jessen, D. H. Petersen, and P. Bøggild, "Graphene antidot lattice transport measurements," Int. J. Nanotechnol. **14**, 226–234 (2017).
[5]S. Y. Chou, P. R. Krauss, and P. J. Renstrom, "Imprint lithography with 25-nanometer resolution," Science **85**, 5258 (1996).
[6]X. Liang, Y.-S. Jung, S. Wu, A. Ismach, D. L. Olynick, S. Cabrini, and J. Bokor, "Formation of bandgap and subbands in graphene nanomeshes with sub-10 nm ribbon width fabricated via nanoimprint lithography," Nano Lett. **10**, 2454–2460 (2010).
[7]D. M. A. Mackenzie, J. D. Buron, P. R. Whelan, B. S. Jessen, A. Silajdźić, A. Pesquera, A. Centeno, A. Zurutuza, P. Bøggild, and D. H. Petersen, "Fabrication of CVD graphene-based devices via laser ablation for wafer-scale characterization," 2D Mater. **2**, 045003 (2015).
[8]B. Luo, J. M. Caridad, P. R. Whelan, J. D. Thomsen, D. M. A. Mackenzie, A. G. Cabo, C. E. Sanders, M. Bianchi, P. Hofmann, P. U. U. Jepsen, P. Bøggild, and T. J. Booth, "Sputtering a reversed metal coating on copper enclosure for large-scale growth of single-crystalline graphene," 2D Mater. **4**(4), 045017 (2017).
[9]B. Luo, P. R. Whelan, A. Shivayogimath, D. M. A. Mackenzie, P. Bøggild, and T. J. Booth, "Copper oxidation through nucleation sites of chemical vapor deposited graphene," Chem. Mater. **28**, 3789–3795 (2016).
[10]A. Shivayogimath, D. Mackenzie, B. Luo, O. Hansen, P. Bøggild, and T. J. Booth, "Probing the gas-phase dynamics of graphene chemical vapour deposition using *in-situ* UV absorption spectroscopy," Sci. Rep. **7**, 6183 (2017).
[11]R. Wang, P. Whelan, P. Braeuninger-Weimer, S. Tappertzhofen, J. Alexander-Webber, Z. Van-Veldhoven, P. Kidambi, B. Jessen, T. Booth, P. Boggild, and S. Hofmann, "Catalyst interface engineering for improved 2D film lift-off and transfer," ACS Appl. Mater. Interfaces **8**, 33072–33082 (2016).
[12]P. R. Whelan, B. Jessen, R. Wang, B. Luo, A. C. Stoot, D. M. A. Mackenzie, P. Braeuninger-Weimer, A. Jouvray, L. Prager, L. Camilli, S. Hofmann, P. Bøggild, and T. J. Booth, "Raman spectral indicators of catalyst decoupling for transfer of CVD grown 2D materials," Carbon **117**, 75–81 (2017).
[13]D. M. A. Mackenzie, J. D. Buron, P. Bøggild, P. U. Jepsen, and D. H. Petersen, "Contactless graphene conductance measurements: The effect of device fabrication on terahertz time-domain spectroscopy," Int. J. Nanotechnol. **138**(8/9), 591–596 (2016).
[14]L. Gammelgaard, J. M. Caridad, A. Cagliani, D. M. A. Mackenzie, D. H. Petersen, T. J. Booth, and P. Bøggild, "Graphene transport properties upon exposure to PMMA processing and heat treatments," 2D Mater. **1**, 035005 (2014).

[15]D. M. A. Mackenzie, J. D. Buron, P. R. Whelan, J. M. Caridad, M. Bjergfelt, B. Luo, A. Shivayogimath, A. L. Smitshuysen, J. D. Thomsen, T. J. Booth, L. Gammelgaard, J. Zultak, and D. Pedersen, "Quality assessment of graphene: Continuity, uniformity and accuracy of mobility measurements," Nano Res. **10**(10), 3596–3605 (2017).
[16]L. van der Pauw, "A method of measuring specific resistivity and Hall effect of discs of arbitrary shape," Philips Tech. Rev. **20**, 220–224 (1958).
[17]M. B. B. Larsen, D. M. A. Mackenzie, J. M. Caridad, P. Bøggild, and T. Booth, "Transfer induced compressive strain in graphene: Evidence from Raman spectroscopic mapping," Microelectron. Eng. **121**, 113–117 (2014).
[18]M. Wang, L. Fu, L. Gan, C. Zhang, M. Rümmeli, A. Bachmatiuk, K. Huang, Y. Fang, and Z. Liu, "CVD growth of large area smooth-edged graphene nanomesh by nanosphere lithography," Sci. Rep. **3**, 1238 (2012).
[19]A. C. Ferrari and D. M. Basko, "Raman spectroscopy as a versatile tool for studying the properties of graphene," Nat. Nanotechnol. **8**, 235–246 (2013).
[20]S. Heydrich, M. Hirmer, C. Preis, T. Korn, J. Eroms, D. Weiss, and C. Schüller, "Scanning Raman spectroscopy of graphene antidot lattices: Evidence for systematic p-type doping," Appl. Phys. Lett. **97**(4), 043113 (2010).
[21]I. Childres, L. A. Jauregui, M. Foxe, J. Tian, R. Jalilian, I. Jovanovic, and Y. P. Chen, "Effect of electron-beam irradiation on graphene field effect devices," Appl. Phys. Lett. **97**(17), 173109 (2010).
[22]A. Cagliani, N. Lindvall, M. B. B. S. Larsen, D. M. A. Mackenzie, B. S. Jessen, T. J. Booth, and P. Bøggild, "Defect/oxygen assisted direct write technique for nanopatterning graphene," Nanoscale **7**(14), 6271–6277 (2015).
[23]F. Withers, T. H. Bointon, M. Dubois, S. Russo, and M. F. Craciun, "Nanopatterning of fluorinated graphene by electron beam irradiation," Nano Lett. **11**(9), 3912–3916 (2011).
[24]E. Llobet, "Gas sensors using carbon nanomaterials: A review," Sens. Actuators B **179**, 32–45 (2013).
[25]M. G. Chung, D. H. Kim, H. M. Lee, T. Kim, J. H. Choi, D. kyun Seo, and Y. H. Kim, "Highly sensitive NO_2 gas sensor based on ozone treated graphene," Sens. Actuators B **166**, 172–176 (2012).
[26]T. O. Wehling, K. S. Novoselov, S. V. Morozov, E. E. Vdovin, M. I. Katsnelson, A. K. Geim, and A. I. Lichtenstein, "Molecular doping of graphene," Nano Lett. **8**, 173–177 (2008).
[27]D. M. A. Mackenzie and S. A. Brown, "Germanium nano-cluster films as humidity and hydrogen sensors," J. Appl. Phys. **112**, 074514 (2012).
[28]S. L. Zhang, H. Jung, J. S. Huh, J. B. Yu, and W. C. Yang, "Efficient exfoliation of MoS2 with volatile solvents and their application for humidity sensor," J. Nanosci. Nanotechnol. **14**, 8518–8522 (2014).
[29]T. Hesterberg, W. Bunn, R. McClellan, A. Hamade, C. Long, and P. Valberg, "Critical review of the human data on short-term nitrogen dioxide (NO2) exposures: Evidence for NO_2 no-effect levels," Crit. Rev. Toxicol. **39**, 743–781 (2009).